

Loose, cohesive granular assemblies: constitutive law and microstructure evolution in quasistatic isotropic compression

Walid Lammali¹, Jean-Noël Roux^{1,*}, Vinh-Du Than¹, and Anh-Minh Tang^{1,**}

¹Lab. Navier, Univ. Gustave Eiffel, École des Ponts, CNRS, 14-20 boulevard Newton, 77427 Champs-sur-Marne, France

Abstract. DEM-simulated cohesive granular materials made of spherical beads of diameter a initially assembled in homogeneous solidlike loose states (solid fraction Φ as low as 20-30%), by ballistic cluster aggregation, are subjected to quasistatic isotropic compression. As the large initial voids gradually collapse under compression, void ratio $e = -1 + 1/\Phi$ decreases irreversibly as in cohesive soils. This plastic compression is controlled by dimensionless ratio $P^* = a^2P/F_0$, comparing pressure P to contact cohesive strength F_0 . The compression curve, e versus $\log P^*$, is sensitive to the initial characteristic velocity during aggregation, which determines network connectivity and microstructure, and to the initial density. Despite the large heterogeneities, this curve is remarkably reproducible, independent of sample size and aspect ratio. Its slope (the compression index) varies with the initial density in the aggregation stage, and, surprisingly, correlates with small scale microstructural features much better than with large scale ones.

1 Introduction

Cohesive granular assemblies, such as powders and colloids, exhibit a wider variety of static states than cohesionless ones. Cohesion may, in particular, stabilize very loose states [1], in which stresses are carried by tenuous, ramified contact networks similar to colloidal gels [2]. Hence interesting compression properties, as initial loose states get irreversibly densified under growing pressure. We report here on a DEM investigation of the response of a simple model material, as presented in Sec. 2, in quasistatic isotropic compression (Sec. 3). While the broad features of the compression behavior were previously reported [1], new results are added here, especially as regards the microstructure (Sec. 4). Sec. 5 presents conclusions.

2 Simulated model

2.1 Particle interactions

The same model system as in Refs. [1, 3] is simulated here: spherical beads of diameter a and mass m , with Hertz contact elasticity, friction coefficient $\mu = 0.3$, and adhesive forces modeling capillary attraction through small liquid menisci, describing wet granular assemblies in the low saturation, pendular regime of isolated liquid bridges. The attractive contact force is simply $F_0 = \pi\Gamma a$ (Γ denoting the interfacial tension of the wetting liquid). This force law has hysteresis: liquid bridges only form in intergranular contacts but survive between receding pairs, which remain in *distant interaction* as long as the separation distance D does not exceed a rupture threshold D_R (here, $D_R = a/10$,

corresponding to meniscus volume $10^{-3}a^3$). Thus, in addition to the contact coordination number, z_c , the distant interaction one, z_d , should also be measured. The attractive force decrease as D grows from zero to D_R is modeled with the simple law of Refs. [1, 3] (“Maugis approximation”). The Coulomb inequality involves the elastic repulsive normal force F_N^e only. A contact with vanishing normal force ($F_N^e - F_0 = 0$) may thus transmit a tangential force as large as μF_0 .

Simulations implementing this simple model agree quantitatively with experimental results in simple shear flow [3, 4], and, semi-quantitatively, in oedometric compression [5].

As in Refs. [1, 3, 4] reduced pressure $P^* = a^2P/F_0$, comparing the adhesive force to pressure P , is used as a dimensionless control parameter. Cohesive effects are strong for small P^* , stabilizing tenuous, open structures [1]. Their influence gradually vanish as P^* increases, until the properties of cohesionless systems are retrieved for large P^* [1, 2].

2.2 Sample preparation

Several samples (4000 to 9000 particles) are prepared for each set of parameters. Simulation cells are triperiodic cubes or tall rectangular cuboids with aspect ratio 2. Loose stress-supporting structures [1, 6] form by ballistic aggregation (without gravity) in a cell of fixed volume. Grains are first randomly placed within the cell, at low solid fraction Φ_0 (e.g., 0.3), without contacts, and given Maxwell-distributed random velocities (mean quadratic velocity V_0). Then, collisions form growing mobile clusters and dissipate kinetic energy. The process stops when a unique, solid, equilibrated cluster, containing all grains, spans the

*e-mail: jean-noel.roux@univ-eiffel.fr

**e-mail: anh-minh.tang@enpc.fr

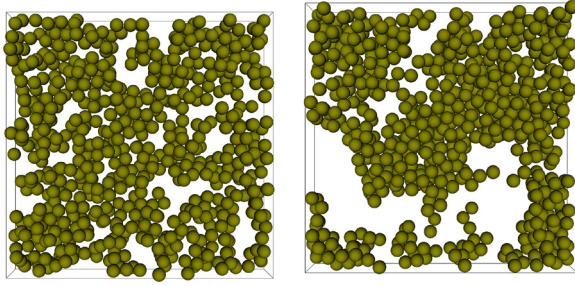


Figure 1. Aspect of aggregated configurations at solid fraction $\Phi_0 = 0.3$ (slices with thickness $3a$ in 4000 grain cubic cells), assembled with $V_0 = V_1$ (left) and $V_0 = V_2$ (right).

system. Its microstructure is determined by Φ_0 and V_0 . V_0 is compared [6] to the escape receding relative velocity V^* from the potential well, for a pair of grains in distant mutual attraction, which writes $V^* \approx 1.3 \sqrt{D_R F_0 / m}$.

Fig. 1 shows structures obtained with $V_0 = V_1 \equiv V^*/5$ and $V_0 = V_2 \equiv 20V^*$, corresponding to the opposite limits of maintained contacts and of strong restructuring during aggregation. Large V_0 values entail heterogeneities (dense regions and pores) on larger scales.

3 Isotropic compression

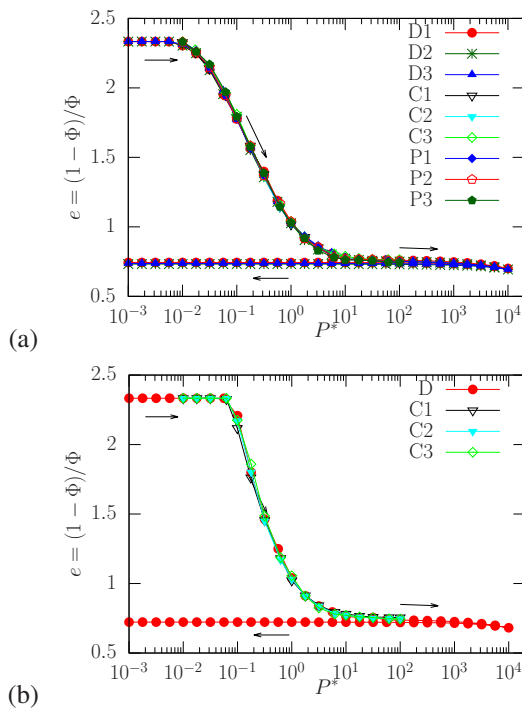


Figure 2. Isotropic compression curve (void ratio versus P^*) of material assembled at $\Phi_0 = 0.3$ with $V_0 = V_1$ (a) and $V_0 = V_2$ (b): cubic samples with 4000 grains (D), and 8788 grains (C), rectangular cuboidal ones (elongated, aspect ratio 2) with 8000 grains (P). Density hardly changes in decompression (see arrows). All results except D in graph (b) are shown for 3 different samples.

Unlike other numerical studies [7], ours deals with *quasistatic* compression, *after* the initial aggregation stage. The initial states of Sec. 2.2 are subjected to step-wise increasing isotropic pressures, while the cell volume decreases to balance the applied load in equilibrated contact networks [2]. The resulting compression curves of Fig. 2, showing void ratio e [8] versus P^* on a logarithmic scale ($e \equiv (1 - \Phi)/\Phi$, with Φ the volume fraction), are remarkably well defined and reproducible, despite the initial heterogeneities (Fig. 1), with no effect of sample size or shape, and surprisingly little sample to sample fluctuations. Irreversible collapse mostly occurs as P^* ranges from 0.1 to a few units (pressures of order 1 kPa for beads with $a = 0.1$ mm wet by water), as the confining pressure gradually dominates capillary cohesion. The evolution of coordination numbers (Fig. 3) exhibits a similar reproducibility. With larger V_0 , better coordinated initial

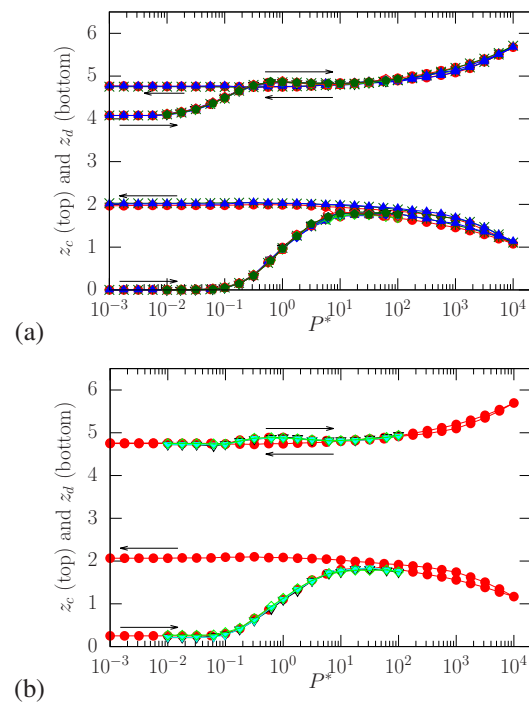


Figure 3. Analogue of Fig. 2 (same symbols and colors) for coordination numbers of contacts (z_c) and of distant interactions (z_d), initial states prepared with $V_0 = V_1$ (a) and $V_0 = V_2$ (b).

states (Fig. 2b) withstand a larger pressure increase before gradually collapsing. With small V_0 , as the forming aggregates do not restructure in the assembling process, z_c (Fig. 3a) starts close to the minimum value 4, and z_d (which counts opening contacts) starts at zero. The material behavior in decompressing from the largest P^* value (under which cohesive effects are negligible), shown in Figs. 2-3, is similar to that of a cohesionless material, with little change in density and coordination number (except at large pressure, due to elastic contact deflections).

The influence of model parameters on material behavior was tested. The force range (meniscus rupture distance D_R) has but a small effect on the isotropic compression curves, which is also hardly affected by a moderate size

polydispersity [5]. Yet, a small rolling (and pivoting) resistance in contacts (crucial in the mechanics of colloidal gels [9]) causes important changes, as even more tenuous networks may be stabilized at low P^* , comprising stress-transmitting thin, one-grain wide strands [5, 6].

The plastic behavior in isotropic compression is similar to that of cohesive soils [8], with a linear variation of the void ratio with $\log P$ in some range. The slope of this curve (known as the *compression index*) depends on the initial microstructure, as apparent on Fig. 2: the plastic compression begins at larger P^* , and occurs faster for the more heterogeneous and better coordinated microstructure prepared with $V_0 = V_2$. The state of minimum void ratio at large P^* , though, is independent of the preparation procedure [1]. Contrarily to the standard presentation of cohesive soil behavior [8] (and to observations in a similar 2D model [2]), the compression index varies with initial solid fraction Φ_0 , as shown in Fig. 4. Interestingly, some states

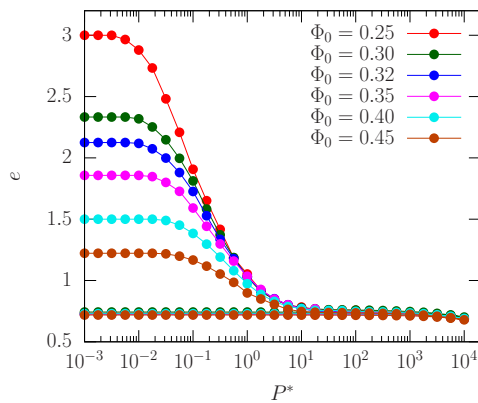


Figure 4. e versus $\log P^*$, as in Fig. 2, for $V_0 = V_1$ and different initial solid fractions Φ_0 (or void ratios $e_0 = 1/(\Phi_0 - 1)$).

assembled with different initial density and different characteristic velocity V_0 may behave similarly, with close values of the compression index in some range. Thus, defining $\Phi_1 \equiv 0.3$ and $\Phi_2 \equiv 0.2$, Fig. 5 shows that preparations with $\Phi_0 = \Phi_1$ and $V_0 = V_2$, on the one hand, and $\Phi_0 = \Phi_2$ and $V_0 = V_1$, on the other hand, have very similar compression curves, the decrease in compression index due to a smaller V_0 compensating the increase caused by a lower Φ_0 . The coincidence (Fig. 5) or difference (Fig. 4) in compression curves and compression indices originates in the preparation-dependent microstructure, as analysed below.

4 Compression law and microstructure

The first internal variables to be measured are the coordination numbers. For different preparations with the same value of V_0 , but different densities, Fig. 6 shows indeed that initially denser samples are less coordinated than initially less dense ones compressed to the same void ratio. Thus they start to yield for lower pressures, whence a lower compression index. Conversely, preparations " Φ_1 - V_2 " (green) and " Φ_2 - V_1 " (red) lead to similar coordination numbers, as shown in Fig. 7, for $e \leq 2.3$, and their

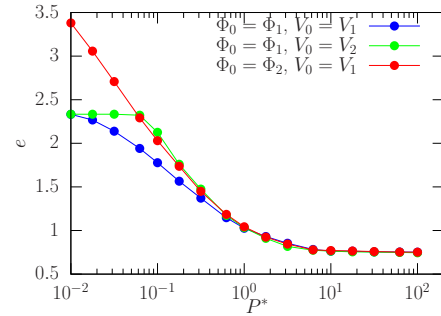


Figure 5. Compression curves for different values of Φ_0 and V_0 (data averaged over 3 independent samples of each kind).

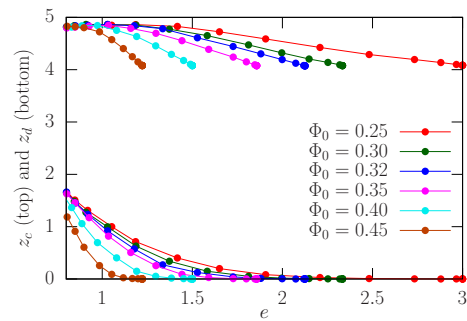


Figure 6. Coordination numbers z_c and z_d versus void ratio (compression proceeds from right to left) for states of Fig. 4 (same color code). Note common z_c value in final dense state [1].

compression curves are also very close. Unsurprisingly,

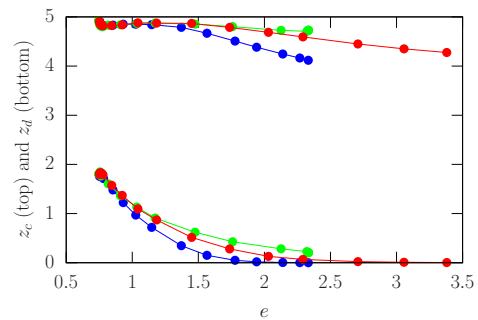


Figure 7. Coordination numbers z_c and z_d versus e for samples of Fig. 5 (same color code).

z_c and z_d thus correlate with plastic compression behavior. Among other small scale features that correlate well with the compression index are the contact angular distributions and the number of triangles and tetrahedra formed by interacting grains.

The complex geometry of loose equilibrated networks should of course be analysed further. It is tempting to try and identify characteristic length scales in loose heterogeneous microstructures (Fig. 1) and correlate them with the compression behavior. We characterise the pore space as follows. To each point \mathbf{x} in the pore space we associate its

minimum distance $D_g(\mathbf{x})$ to a spherical grain surface. D_g values are computed by a Monte-Carlo approach, by repeating a large number (10^7) of random drawings of points in the pore space. Fig. 8 is a plot of the cumulative distribution function (CDF) of D_g over the pore space, growing from 0 to 1, at the initial void ratio 2.33 for choices $V_0 = V_1$ and $V_0 = V_2$. In the more heterogeneous state of

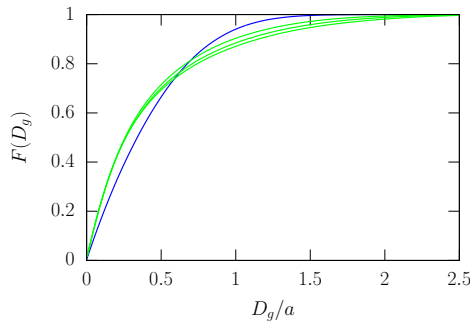


Figure 8. CDF of distances D_g (in units of a) in void space for initial states with $\Phi_0 = 0.3$, assembled with $V_0 = V_1$ (blue) and $V_0 = V_2$ (green, 3 samples).

type " Φ_1-V_2 " (green), the largest D_g values approach 3: the void space contains a few spheres of diameter $6a$. A few percent of the void space is at distance larger than $2a$ from the grain surfaces. Meanwhile, small values $D_g \leq a/2$

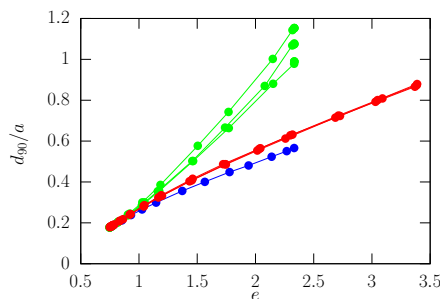


Figure 9. Distance d_{90} versus void ratio e in compression. Same color code as in Fig. 5 (3 samples for red and green curves).

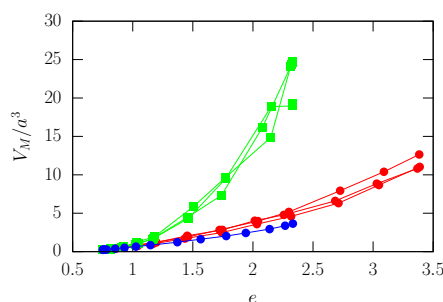


Figure 10. Analogue of Fig. 9 for mass-averaged pore volume V_M (same samples and color code).

are also more frequent, evidencing larger dense clusters

than for states " Φ_1-V_1 " (blue). Defining distance d_{90} by $F(d_{90}) = 0.9$ (such that 90% of the volume of voids is closer to a grain surface), its variations are represented in Fig. 9 for the three compression curves of Fig. 5. The marked difference between red and green curves on this graph signals that the compression behavior does not correlate with length d_{90} associated with large cavities.

We split the void space into different pores using an "inflating bubble" algorithm (this is equivalent to the Delaunay construction approach, if pores are merged when their separating constriction radius is larger than that of their central cavity). The resulting mass-averaged pore volume, V_M , is shown for the same states in Fig. 10. While for $e \leq 2.3$ the compression curves for initial states " Φ_1-V_2 " (green) and " Φ_2-V_1 " (red) are very close, average pore size V_M values strongly differ, like those of d_{90} . Thus, somewhat counter-intuitively, large density heterogeneities do not determine the compression behavior. This may explain the excellent reproducibility of the compression curves, whereas sample to sample fluctuations are apparent in the large scale variables shown in Figs. 8 to 10.

5 Conclusions

Our simulations thus show the model cohesive material to possess a very well defined constitutive law in compression, with e versus $\log P^*$ curves akin to those of cohesive powders or soils. The compression law is sensitive to the initial state density and microstructure. The large scale features of loose states (associated to pores and dense regions) are surprisingly little correlated to the compression index, which is apparently determined by small scale characteristics like connectivity. Other relevant state parameters could be searched for. Our study provides a basis for comparisons with similar loose cohesive states as obtained by other preparation methods, experimentally or numerically, and a wide range of loose microstructures with varying mechanical properties has yet to be explored.

References

- [1] V.D. Than, S. Khamseh, A.M. Tang, J.M. Pereira, F. Chevoir, J.N. Roux, *ASCE Journal of Engineering Mechanics* **143**, C4016001 (2017)
- [2] F.A. Gilabert, J.N. Roux, A. Castellanos, *Phys. Rev. E* **78**, 031305 (2008)
- [3] M. Badetti, A. Fall, F. Chevoir, J.N. Roux, *European Physical Journal E* **41**, 68 (2018)
- [4] M. Badetti, A. Fall, D. Hautemayou, S. Rodts, J.N. Roux, *J. of Rheology* **62**, 1175 (2018)
- [5] V.D. Than, Ph.D. thesis, Université Paris Est (2017)
- [6] F.A. Gilabert, J.N. Roux, A. Castellanos, *Phys. Rev. E* **75**, 011303 (2007)
- [7] M. Sonzogni, J.M. Vanson, K. Ioannidou, Y. Reynier, S. Martinet, F. Radjai, *Soft Matter* **20**, 5296 (2024)
- [8] J. Mitchell, K. Soga, *Fundamentals of Soil Behavior* (Wiley, 2005)
- [9] F. Bonacci, X. Chateau, E.M. Furst, J. Goyon, A. Lemaitre, *Phys. Rev. Lett.* **128**, 018003 (2022)